University of Huddersfield Repository

Hinks, J. A., Haigh, S. J., Greaves, Graeme, Sweeney, Francis, Pan, C. T., Young, R. J. and Donnelly, S. E.

Dynamic Microstructural Evolution of Graphite under Displacing Irradiation

Original Citation

This version is available at http://eprints.hud.ac.uk/id/eprint/19098/

http://eprints.hud.ac.uk/

Accepted Manuscript

Dynamic Microstructural Evolution of Graphite under Displacing Irradiation

J.A. Hinks, S.J. Haigh, G. Greaves, F. Sweeney, C.T. Pan, R.J. Young, S.E. Donnelly
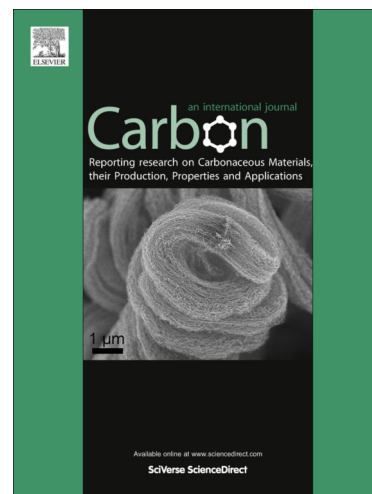
Dynamic Microstructural Evolution of Graphite under Displacing Irradiation

J.A. Hinks [a], S.J. Haigh [b†], G. Greaves [a], F. Sweeney [a], C.T. Pan [b,c], R.J. Young [b], S.E. Donnelly [a]*

[a] *School of Computing and Engineering, University of Huddersfield, HD1 3DH, United Kingdom*

[b] *School of Materials, University of Manchester, Material Science Centre, Grosvenor Street, Manchester, M13 9PL, United Kingdom*

[c] *School of Physics and Astronomy, University of Manchester, Manchester M13 9PL, United Kingdom*

Abstract

Graphitic materials and graphite composites experience dimensional change when exposed to radiation-induced atomic displacements. This has major implications for current and future technological ranging from nuclear fission reactors to the processing of graphene-silicon hybrid devices. Dimensional change in nuclear graphites is a complex problem involving the filler, binder, porosity, cracks and atomic-level effects all interacting within the polygranular structure. An improved understanding of the atomistic mechanisms which drive dimensional change within individual graphitic crystals is required to feed into the multiscale modelling of this system.

In this study, micromechanically exfoliated samples of highly oriented pyrolytic graphite have been ion irradiated and studied *in situ* using transmission electron microscopy (TEM) in order to gain insights into the response of single graphitic crystals to displacing radiation. Under continuous ion bombardment, a complex dynamic sequence of deformation evolves featuring several distinct stages from the inducement of strain, the creation of dislocations leading to dislocation arrays, the formation of kink band networks and localised doming of

---

[*] *Corresponding author at:* School of Computing and Engineering, University of Huddersfield, HD1 3DH, United Kingdom
E-mail address: j.a.hinks@hud.ac.uk

[†] *Corresponding author at:* School of Materials, University of Manchester, Material Science Centre, Grosvenor Street, Manchester, M13 9PL, United Kingdom
E-mail address: sarah.haigh@manchester.ac.uk

the sample. Observing these ion irradiation-induced processes using *in situ* TEM reveals previously unknown details of the sequence of microstructural developments and physics driving these phenomena. A mechanistic model consistent with the microstructural changes observed is presented.

1.   Introduction

The response of graphene and other graphitic materials to radiation-induced atomic displacements is poorly understood despite the large number of technological and industrial applications upon which it impacts. For example, polycrystalline graphite composite materials are used in current nuclear fission reactors such as Advanced Gas-cooled Reactors (AGRs) [1] and are proposed for use in Generation IV (GenIV) reactor designs including the Very-High Temperature Reactor (VHTR) and Molten Salt Reactor (MSR) [2]. Current nuclear fission reactors typically expose core components to radiation damage levels up to the order of 10 Displacements Per Atom (DPA) [3] with GenIV increasing this up to 200 DPA over the expected operational lifetimes [2]. In order to produce the safety case for the extension of the operational lifetime of existing nuclear power stations and to develop materials for future reactor designs, it is important that the effects of displacing radiation be better understood. The deployment of graphene nanocomposite materials [4–6] in extreme environments is highly desirable but their safe use will require an understanding of the damage mechanisms in these materials. Furthermore, the successful development of graphene-based heterostructures for integrated electronics [6–8] will rely on the radiation stability of these devices both during processing and whilst in service.

One of the key challenges for both functional and structural applications of graphitic materials is radiation damage and in particular the known phenomenon of dimensional change under displacing irradiation. In nuclear graphite, this is a multiscale problem requiring the consideration of atomic-level effects as well as the filler, binder, porosity and cracks all interacting within the polygranular structure. In both the polygranular and single-crystal cases, the resulting dimensional changes can be significant in terms of the magnitude and tre implications for materials applications.

At the single-crystal level, dimensional change consists of a contraction in the a/b-directions (i.e. in the basal planes) and an expansion in the c-direction (i.e. normal to the basal planes) [9–13]. The atomistic mechanisms which give rise to these changes are the subject of debate and the focus of considerable on-going scientific research [14–16]. One proposed theoretical model, which we refer to as the "Point Defect" model, suggests that radiation-

2

induced vacancies agglomerate in the graphene sheets to form small dislocation loops. These then collapse causing contraction in the a/b-directions with expansion in the c-direction attributed to the agglomeration of interstitials between the basal planes to form new layers [17,18]. More recent atomic-level models of defects in graphite and graphene offer alternative possibilities for the contraction of the basal plane in the form of 5- and 7-member rings [19–24] or the rucking of the basal planes due to dislocation motion [14]. However, none of these models has been conclusively verified by experiment.

Considerable insight into the response of a material to displacing irradiation and, in particular, into the formation, evolving morphology and behaviour of extended defects can be obtained by performing *in situ* ion and/or electron irradiation studies within a Transmission Electron Microscope (TEM). The use of such techniques has made important contributions to understanding in areas such as the effects of ion-induced collision cascades on extended defects [25] and surfaces [26], the effects of fluxes of point defects on precipitates in metals [27], nanocluster ejection [28,29] and the development of amorphous zones in silicon [30].

To date, however, the majority of work on microstructural radiation damage in graphite has been confined to *ex situ* analysis of neutron (for examples see [31–35]) and ion (for examples see [36–40]) irradiated material with only a small number of studies using TEM with *in situ* ion [41–45] and electron [15,46–48] irradiation. Radiation damage is a complex dynamic process in which multiple mechanisms compete to determine the ultimate outcome. It is necessary to observe the system *in situ* whilst under irradiation in order to capture its evolution rather than to examine only the end-state accessible in *ex situ* studies. In this paper we report *in situ* TEM observation of the dynamic sequence of structural changes that occur as a result of ion irradiation induced mechanical deformation behaviour of a single graphitic crystal.

The purpose of this work is to provide a better understanding of the underlying mechanisms that give rise to the known phenomenon of dimensional change in single-crystal graphite. This would provide useful knowledge to inform a full multi-scale model of polygranular nuclear graphite, which would also need to consider the behaviour of grain boundaries, filler, binder, cracks and porosity under displacing irradiation. The work has direct application to the understanding of radiation damage in graphene-silicon heterostructures.

3

2.   Experimental Methods

2.1   Sample preparation

Samples of thin graphite were produced by micromechanical cleavage of highly-orientated pyrolytic graphite (HOPG). Suitable flakes were identified using an optical microscope to observe the contrast produced by the flakes deposited on a silicon wafer with a ~90 nm SiO_2 surface oxide [49,50]. A 200 nm poly(methyl methacrylate) (PMMA) layer was then spin-coated on top. The flakes were detached from the silicon substrate by soaking in 3% potassium hydroxide for a few hours at room temperature to dissolve the SiO_2. The samples were then rinsed in deionised water and transferred to TEM grids. Finally, the PMMA was dissolved with acetone and the TEM grids with free-standing graphite were dried in a critical-point dryer. Further details of the sample preparation techniques have been reported previously [51,52].

The TEM samples produced in this way featured electron-transparent large single crystals of graphite with lateral dimensions typically of 10–100 μm. The single crystal TEM diffraction data and lack of Moiré fringes under TEM observation indicated the absence of rotational misorientation between the basal planes. Raman spectroscopy was performed on some samples using a Renishaw 1000 Raman Spectrometer with a 514 nm wavelength laser and ~2 μm spot size. The samples were found typically to be free from significant levels of defects and dopants as indicated by the absence of a prominent D peak in the Raman spectra [53–55].

It was vital to use high quality single crystals for this work to allow the clear observation and interpretation of features such as diffraction contrast due to the strain fields around dislocations. In more-polycrystalline graphite samples the contrast can be dominated by twist dislocations and/or Moiré patterns due to rotational misorientation between the basal planes. In nuclear graphites, the inhomogeneous polygranular structure of those materials similarly makes definitive identification and analysis of defects problematic in many cases. Whilst the single crystals used in this work offer the clear advantage of suitable crystallographic orientation and the absence of obfuscating contrast in the TEM, they are relatively-simple systems and thus extrapolation to the more complex case of nuclear graphite must be undertaken with caution. These are good model systems in which to explore the dynamic processes which can occur in single crystallites but do not contain features such as filler and binder phases, cracks and porosity which play significant roles in radiation induced dimension change in polygranular nuclear graphite. Therefore it is the aim of the current study to explore

the atomistic and single-crystal level effects to feed into a better understanding of the multiscale problem of radiation induced dimensional change in nuclear graphite. However, the samples used in the current study are directly comparable to materials used in technologies which utilise single crystals of graphitic material such as graphene-based heterostructures for integrated electronics.

2.2   *Transmission electron microscopy with* **in situ** *ion irradiation*

TEM with *in situ* ion irradiation was performed using 60 keV Xe^+ ions at room temperature in the Microscope and Ion Accelerator for Materials Investigations (MIAMI) facility at the University of Huddersfield which is described in detail elsewhere [56]. At this energy around 30% of the Xe will have been stopped in the TEM sample but at the low fluences used the effect of this amount of inert gas is expected to be negligible as discussed below in section 3.5.3. A low ion beam flux of 5×10^{10} ions cm^{-2} s^{-1} was chosen to prevent any sample heating and consequent thermal-shock effects. The JEOL JEM-2000FX TEM used for the *in situ* MIAMI experiments was operated at 80 kV to minimise the known damaging effects of electron beam irradiation of graphitic materials [15,48,57]. Any significant contribution of the electron beam to the observed effects was ruled-out by comparison of the areas of the samples followed during the experiments to those not exposed to the electron beam. Video was captured using a Gatan ORIUS SC200 camera at a frame rate of 8 s^{-1} and recorded digitally using a frame size of 480×480 pixels. Additional experiments were performed at the MIAMI facility using either 30 keV He^+ or 30 keV Ar^+.

2.3   *Electron microscopy* **ex situ** *analysis*

Post-irradiation High Resolution TEM (HRTEM) imaging was performed using a Tecnai F30 TEM operating at 300 kV. Scanning Electron Microscopy (SEM) imaging was performed using a FEI Quanta 250 fitted with a field emission gun and operating at 30 kV.

2.4   *Monte Carlo calculations of ion transport in graphite*

Damage profiles, implantation and atomic displacement values were calculated with the *Stopping and Range of Ions in Matter* (SRIM) Monte Carlo computer code version 2013 [58] using a displacement energy, E_d, of 28 eV, a target thickness of 25 nm, a target density of 2.253 g cm^{-3} and an incident ion angle of 30° to the surface normal in accordance with the geometry during the *in situ* ion irradiations. Calculations for other experimental geometries referenced in the discussion were performed with appropriate adjustments.

3.   Results and Discussion

3.1   *Damage profile of 60 keV Xe⁺ ions in graphite*

For a graphite sample 25 nm thick (equivalent to 74 basal planes), 60 keV Xe^+ ions incident at 30° from the surface normal (the conditions used in the experiments reported here) will create a highly non-uniform damage profile. As illustrated in Fig.1a, Displacement Per Atom (DPA) levels peak at a depth of around 17.5 nm. Dimensional change in graphite is known to be related to the DPA [1,9–12] and will therefore vary in a similar manner as a function of sample depth. Fig. 1b shows a schematic illustration of the dimensional change in the a/b-directions that this damage profile would produce for an unconstrained system in the absence of interplanar forces, pre-existing grain structure, any surrounding material or other external forces. In practice, these influences cannot be ignored and the deformation behaviour resulting from radiation induced atomic displacements is far more complex.
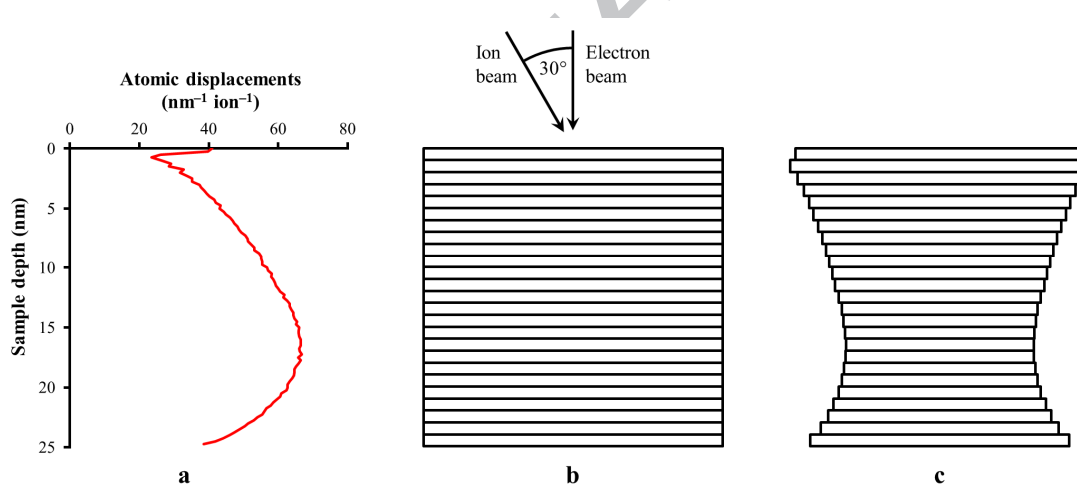
Fig. 1 – Depth dependence of the number of ion irradiation induced atomic displacements and dimensional change in a thin graphite crystal: (a) the number of atomic displacements per incident ion as a function of sample depth for 60 keV Xe⁺ ion irradiation as calculated using SRIM; (b) schematic representation of layers in the virgin material showing the geometry of the sample relative to the electron and ion beams in the *in situ* experiments reported here; and (c) schematic representation of irradiation-induced contraction in a/b directions in the absence of any interplanar forces, grain structure or other constraints and neglecting c-axis expansion.

3.2   Transmission electron microscopy in situ observations of ion irradiation

3.2.1   Dynamic evolution of microstructure

The TEM micrographs in Figs. 2a–d show the structural changes observed in a single crystal of graphite during the *in situ* experiments as observed perpendicular to the basal planes. These images were extracted from video captured during continuous ion irradiation which allowed the evolution of this dynamic system to be recorded. Videos are available online in supplementary material. Also in Fig. 2 are schematic diagrams illustrating the microstructure of the sample at each stage of the process as it would appear if viewed parallel to the basal planes. The relative ion fluences for each micrograph and the expected DPA at depths of 1.0 and 17.5 nm are shown in Fig. 2e.
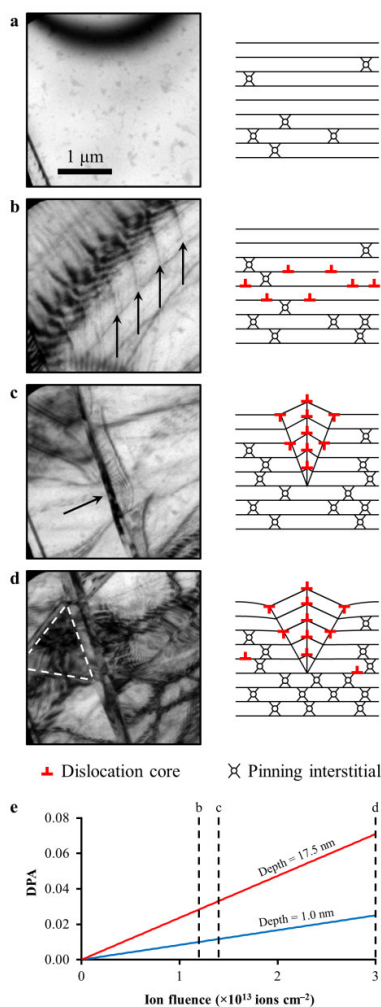
Fig. 2 – Radiation induced structural modification and evolution in a thin single crystal of graphite observed perpendicular to the basal planes via TEM during *in situ* ion

7

irradiation with 60 keV Xe$^+$ ions at room temperature (videos available online in supplementary material): (a) virgin sample before ion irradiation; (b) an irradiation-induced dislocation array (indicated by black arrows) at a fluence of 1.2×10^{13} ions cm^{-2}; (c) immediately after the creation of kink bands (example indicated by black arrow) at a fluence of 1.4×10^{13} ions cm^{-2}; (d) at the end fluence of 3.0×10^{13} ions cm^{-2} showing the 60° orientation relationship between kink bands (indicated by dashed white equilateral triangle); (a)–(d) schematic diagrams illustrating the evolution of the microstructure viewed parallel to the basal planes (see text for further discussion); and (e) graph showing comparative DPA levels against ion fluence at sample depths of 1.0 and 17.5 nm with the relative positions on the fluence axis corresponding to micrographs (b)–(d) indicated. The micrographs show the same area of the sample and the scale marker in (a) applies to all four micrographs.

3.2.2 *Low ion fluence effects*

At low ion irradiation fluences (0 to 3×10^{12} ions cm^{-2}), no significant structural changes were observed except for movement of bend contours – an example of such a contour is shown in Fig. 2a. Even during these early stages of irradiation, significant numbers of both vacancies and interstitial atoms are created and the non-uniform damage profile produced internal stresses in the material as basal planes in the lower region of the sample attempted to contract at a faster rate than those in the upper region.

3.2.3 *Dislocation array formation*

At a fluence of 3.3×10^{12} ions cm^{-2}, basal dislocations began to be injected into the sample from the grain boundary in the lower left-hand corner of the micrographs in Fig. 2. The creation of these dislocations can be understood in terms of the requirement to accommodate more atoms per unit area of basal plane in the upper region of the sample relative to those in the lower region. As these dislocations will be of the same sign they exert a repulsive force on each other with the injection of each additional dislocation causing the existing dislocations to move in order to maintain an equilibrium separation. In this way, equally spaced dislocations were caused to process across the grain forming a dislocation array as shown in Fig. 2b. A video of the formation of this dislocation array is available online in the supplementary material. As can be seen in the video, the movement of the dislocations was not a smooth, continuous motion but progressed in discrete steps as the dislocations became repeatedly snagged and freed as they interacted with pinning sites in the crystal [59–62]. Ordered

8

dislocation arrays have been seen previously in graphite [63–67] but this is the first report of the observation of a dynamic process which leads to the formation of such structures.

The dislocations are unlikely to have formed from the agglomeration of interstitials as discussed below in section 3.5.1. In order for a basal dislocation to exist in graphite, two adjacent basal planes must have different lengths in the direction normal to the dislocation line. This can be achieved by a row of atoms being either inserted into, or removed from, one of the basal planes. As the basal planes contracted at greater rates in the lower portion of the sample, a corresponding number of dislocations were necessarily created in the upper portion.

At a fluence of 1.4×10^{13} ions cm^{-2}, the diffraction conditions changed abruptly causing the contrast associated with the dislocation array to be reduced for a period of 7 s, equivalent to an additional fluence of 3.5×10^{11} ions cm^{-2}. However, during this period the array was still visible with reduced contrast but with apparently the same arrangement of defects. This suggests that the change was due to an event elsewhere in the sample and/or at the interface with the support grid. This then caused a slight adjustment in the local crystallographic orientation and thus diffraction conditions rather than the changes observed being due to a reordering of the defects in the local area under observation.

3.2.4 Kink band formation

Shortly afterwards at the same nominal fluence of 1.4×10^{13} ions cm^{-2}, the dislocation array was suddenly replaced by a network of kink bands as shown in Fig. 2c in a transition that occurred in less than one video frame (< 0.125 s). The symmetry of the kink band network reflected that of a <0001> zone axis in graphite with the kink bands orientated at 60° to each other as highlighted by the dashed white equilateral triangle in Fig. 2d. The axis of the largest of these kink bands was parallel to the preceding dislocation array shown in Fig. 2b and thus also to the grain boundary from which the dislocations were injected. Kink bands are similar to twin boundaries except that the crystallographic orientation is less well defined and have been observed in graphite subjected to mechanical stress [68] and ion irradiation [40,45,69].

As the dislocation density increased prior to kink band formation, the total energy associated with the dislocations would have also increased until it became energetically favourable for buckling of the upper graphene sheets to occur creating a kink band. Kink bands formed in this way occur only when internal stresses reach a level such that the dislocation separation becomes less than a critical value. Below this critical defect separation, the dislocations attract and it becomes energetically favourable for them to align vertically to form a kink boundary as shown in the transition from Fig. 2b to Fig. 2c.

9

3.2.5 Effects of continued ion irradiation

Under continued ion irradiation, the width of the largest kink band as measured in projection increased at a rate of approximately 0.6 nm s^{-1} as shown in Figs. 2c and 2d. This indicates that the newly-formed boundaries are glissile and allow the continuous differential dimensional change to be accommodated through an increased amount of 'kinking' to the grain structure. The kink regions continued to increase in width until ion irradiation was ceased after a fluence of 3.0×10^{13} ions cm^{-2} to allow further *ex situ* analysis of the irradiated sample.

After ion irradiation was stopped, the dislocations continued to move for a period of time as the microstructure relaxed. However, given the calculated migration energy for vacancies and interstitials (see section 3.5.1 below), point defect activity would have been confined to the recombination and agglomeration of close-pairs. Residual strain in the sample will have provided a driving force for dislocation motion which was punctuated by interaction with the established population of pinning sites on which the dislocations became repeatedly snagged and then freed. The rate of microstructural change was observed to decrease to a relatively slow rate over a period of around 600 s.

3.3 Surface morphology of kink bands
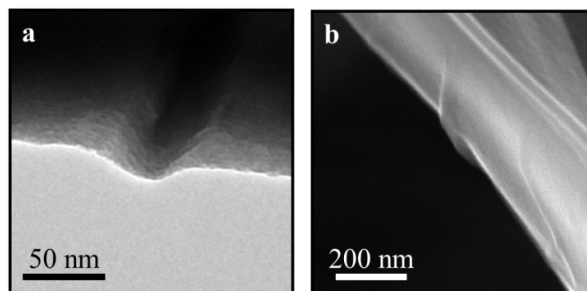
Fig. 3 – Radiation induced kink bands in graphite: (a) *in situ* TEM and (b) *ex situ* SEM images of kink bands on the 60 keV Xe$^+$ ion irradiated surface of graphite where the sample has buckled outwards in order to accommodate ion beam induced dimensional change within the material. The regions shown correspond to the edge of a thin TEM foil where the graphite has curled such that the basal planes have become orientated parallel to the imaging electron beam.

Fig. 3 shows TEM and SEM images of the post-irradiation structure demonstrating the magnitude of the out-of-plane buckling. The kink bands can be most clearly seen to protrude out of the basal plane where the thin graphite has curled at the edge of the TEM samples. Kink bands were detected only on the upper surfaces – i.e. on the surface on which the ion beam was incident. Analysis reveals the out-of-plane rotation at either side of the kink band shown in Fig. 3a to be approximately 21° and 26° neglecting parallax. This is compared to a perfect twin boundary which has a rotation angle of 20.8° about the $<1\bar{1}00>$ direction [70,71].

3.4 *Further analysis of kink band networks and bend contour patterns*

Repeat experiments have demonstrated that these results are reproducible with similar sequences of irradiation induced microstructural changes observed. Under appropriate diffraction conditions, six fold star-shaped features in the centre of the grains are observed to be created as a consequence of dislocation arrays and kink band network formation. These are zone-axis patterns produced by the intersection of {-1 1 0 0} bend contours at a <0 0 0 1> zone axis and indicate regions of the sample where ion irradiation induced strain has caused the surface of the sample to become locally domed. Similar features have been observed previously in *ex situ* studies of neutron irradiated graphite [34] but here we present the first evidence of the dynamic mechanisms which lead to their creation.
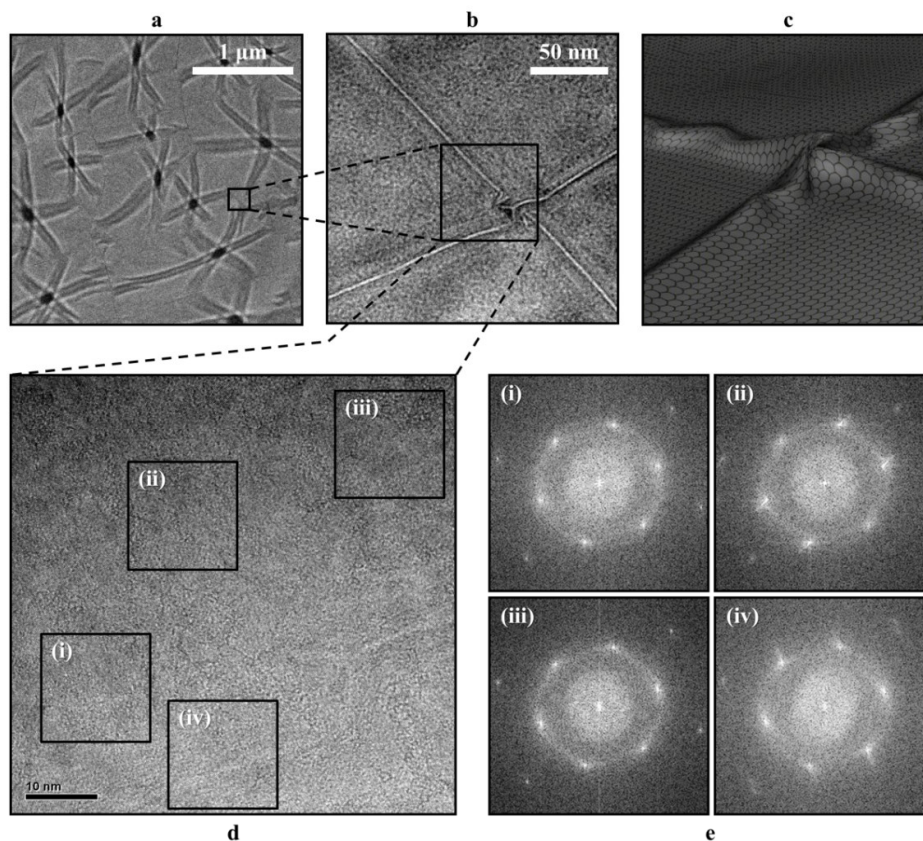
Fig. 4 – Dislocations and star-shaped bend contour patterns induced in a thin graphite sample by 30 keV Ar$^+$ ion irradiation: (a) bright field TEM micrograph showing a distinctive network of bend contours caused by the radiation-induced doming of the sample; (b) bright field TEM micrograph acquired at an underfocus of 300 nm of the region indicated in (a) showing the topographic structure of the intersection between the two line defects; (c) computer generated visualisation showing the intersection of two dislocation creases and demonstrating how the structure shown in panel (b) could arise; (d) HRTEM micrograph of area indicated in (b); (e) comparison of FTs taken from regions either side of the line defects (see (i) and (iii)) with those performed across the defects themselves (see (ii) and (iv)) featuring streaking perpendicular to the defects in the latter two FTs indicative of local distortion associated with these features.

The most striking example of these star features has been observed in a complementary *in situ* TEM experiment using 30 keV Ar$^+$ ions which creates a similar damage profile to the 60 keV Xe$^+$ case. Post-irradiation HRTEM analysis is presented in Fig. 4 with Fig. 4d showing a lattice-resolution image of a region where two line defects intersect. Local Fourier Transforms (FTs) performed on either side of the defect reveal no change in the orientation of the graphite

lattice. However, FTs from regions of the image containing the line defects themselves demonstrate streaking of the lattice spots perpendicular to the line. For the line defect running top-to-bottom in Fig. 4d, the (–1 0 1 0) and (–1 1 0 0) reflections are streaked along the [–2 1 1 0] direction as shown in Fig. 4d(ii) and for the defect that runs left-to-right the (0 –1 1 0) and (–1 0 1 0) reflections are streaked along the [–1 –1 2 0] direction as shown in Fig. 4d(iv). This feature of the FTs is consistent with an array of basal dislocations which have dissociated into partials separated by a local stacking fault [65] and indicates significant levels of distortion in these regions of the sample.

A dislocation in a graphene sheet at a surface is highly analogous to the classic model of a dislocation as a ruck in a rug which is often attributed to Orowan [72]. The structure which can be seen in Fig. 4b can be understood by considering the interaction of two such dislocations. Fig. 4c is a computer generated visualisation illustrating how the intersection of two orthogonal rucks can generate the type of structures observed in HRTEM.

Structural defects can lead to out-of-plane buckling of graphene [19,20] as unconstrained two-dimensional materials can convert in-plane elastic energy into bending energy by relaxing into the third dimension. Such behaviour has been predicted by molecular dynamics [21,73], *ab initio* calculations [24] and continuum theory [74] to occur at dislocations and grain boundaries. Buckling has been observed experimentally in graphene via HRTEM [75], scanning tunnelling microscopy [76], atomic force microscopy [23]. Although the thin graphite samples used in the current study are too thick to be considered two-dimensional (i.e. graphene), the first and last basal planes are free to relax out-of-plane provided they are not prevented from doing so by pinning to the neighbouring basal plane. Therefore, it is possible that a similar relaxation process has occurred in the topmost basal plane in Fig. 4. Further work is underway to understand the structure of both these features and the kink bands shown in Figs. 2 and 3.

3.5   *Possible theoretical explanations for observed phenomena*

3.5.1   *Point defect agglomeration*

The response of materials to radiation damage is complex and varies as a function of temperature, particularly in terms of defect mobility. Recent theoretical calculations put the migration energy of vacancies ($E_{m,v}$) in graphite at 1.0 eV [77] to 1.1 eV [78] although it should be noted that other studies have attributed higher values in the range 1.3–1.7 eV [18,79–82]. At 1.0 eV, vacancy jump rates of 1 Hz are achieved at around 100°C assuming a

vibrational frequency parallel to the basal planes of $5{\times}10^{13}$ Hz [59]. The latest calculations for the migration energy of interstitials ($E_{m,i}$) give values between 1.2 eV [83] and 2.1 eV [82] which equate to interstitial jump rates of about 1 Hz at 170°C and 500°C, respectively. Point-defect clusters (so-called "black spot" damage) are observed in irradiated graphite. However, this only develops into dislocation loops through the migration of point defects if annealed or irradiated at temperatures reported in the literature as being at least 650°C for vacancy-type defects [66] and 900°C for interstitial-type defects [33,84,85].

A small amount of thermal energy is imparted to the volume affected by the atomic collision cascade in its thermal phase but this rapidly dissipates over timescales on the order of 10^{-11} s facilitating only limited enhancement to point defect migration. Therefore in the room temperature experiments reported here, vacancy mobility would have been very limited and the role of the irradiation-induced interstitials would have been confined to interlayer pinning.

On the basis of the migration energies of vacancies and interstitials in graphite and the reported temperatures required for dislocation loop growth, the dislocation and kink band formation observed at room temperature is unlikely to be explained by point defect agglomeration. Further experimental work is underway to explore the effects of temperature on the dynamic microstructural evolution of graphite under the same displacing irradiation conditions reported in the current work.

3.5.2 *Electronic excitation effects*

The formation of kink bands by 20 keV He[+] ion irradiation has been reported by Muto *et al* [45]. In that study, as the energy loss of the He^{+} ions due to electronic stopping was greater in the near-surface region of the sample than at greater depths, the mechanism for the formation of structures on the irradiated surface was tentatively attributed to electronic excitation effects. We have performed similar experiments with 30 keV He[+] ion irradiation in which we observe basal plane contraction but no dislocation or kink band formation despite the greater electronic stopping at this higher energy.

For the energy and sample thickness combination used in our He^{+} ion irradiation experiments, the damage profile was relatively uniform across the depth of our samples. However, for 20 keV He[+] ion irradiation of the 100 nm thick samples used in the study by Muto *et al*, the damage profile would have been very similar to that in our 60 keV Xe[+] ion irradiation experiments reported here. Therefore there would have been significantly more atomic displacements (and hence basal plane contraction) in the bottom of the sample relative

to the top and thus similar mechanisms to those proposed in the current paper could have occurred.

In collective analysis of both the current work and that of Muto *et al*, there is no consistent correlation between kink band formation and electronic stopping in the near-surface. However kink band formation is consistently observed under experimental conditions which produce non-uniform damage profiles. Therefore, it is concluded that the previously proposed electronic excitation mechanism is unlikely to be a major driver for kink band formation but the possibility that it plays a minor role cannot be excluded.

### 3.5.3 *Xe bubble formation leading to surface blistering*

Inert gas bubbles form as a consequence of ion implantation at different fluences depending on experimental factors including ion species, ion energy, target composition and temperature. For example in silicon at room temperature, ion irradiation results in the nucleation of bubbles at around 5×10^{16} ions cm^{-2} for 6 keV He^+ [86] and 5×10^{15} ions cm^{-2} for 80 keV Xe^+ [87]. For these conditions, SRIM calculations predict the peak concentration of the implanted species at nucleation to be approximately 6×10^{21} cm^{-3} and 2×10^{21} cm^{-3}, respectively. Bubble nucleation, growth and consequential intersection with a surface can lead to blistering and thus significant microstructural changes [88]. However, at the end fluence of the experiments reported here the peak gas concentration calculated by SRIM is only 2×10^{19} cm^{-3}. Furthermore, the implantation profile is peaked towards the back of the sample with no Xe calculated to stop within the first 10 nm and thus near the surface on which microstructural features were observed.

In graphite, there is no data in the literature regarding the nucleation fluence for ion irradiation induced Xe bubbles. However, He agglomerations have been observed in graphite at fluences as low as 10^{15} to 5×10^{15} ions cm^{-2} in experiments performed at the higher temperatures of 100–700°C with 25 keV He^+ ion irradiation [69]. The development of large lenticular bubbles has been observed to occur for room temperature implantation of pyrolitic graphite with 40 keV He ions with blister formation and flaking observed for implantation at 500°C [89]. However, the fluences in that work were $1–2 \times 10^{17}$ ions cm^{-2} with a peak helium concentration estimated by the authors to be in excess of 10 at-%. This compares to an estimated peak Xe concentration in the present work of only 0.02 at-%.

The low gas concentration combined with the absence of any TEM observations of Xe bubbles in our experiments (in which we expect to resolve bubbles ≥ 1 nm in diameter) leads to the conclusion that Xe bubble formation and particularly surface blistering can be ruled out

15

as driving mechanisms for the microstructural evolution. This is in line with observations by Bacon and Rao [90] of similar deformation of pyrolitic graphite under He irradiation where they concluded that the gas retained did not appear to play an important role.

3.6   *Implications for the Point Defect model*
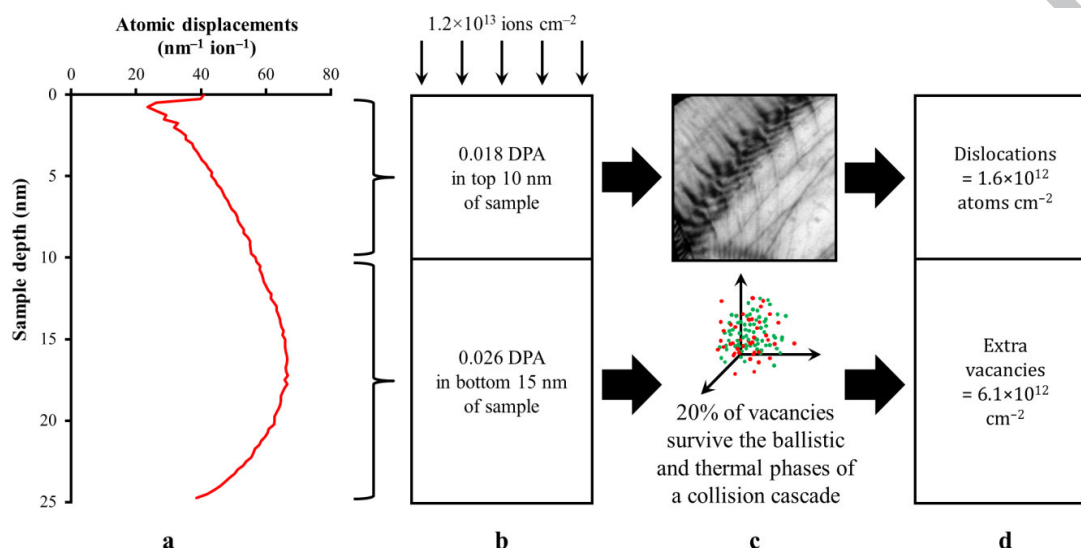
Fig. 5 – Comparison of expected point defect populations with experimental observations for 60 keV Xe$^+$ ion irradiation of graphite: (a) atomic displacements per ion as function of sample depth; (b) DPA levels in top 10 nm and bottom 15 nm of sample at a fluence of 1.2×10^{13} ions cm^{-2}; (c) dislocation density observed at this fluence (top) and typical MD simulation result (bottom) that 20% of vacancies will survive the ballistic and thermal phases of a collision cascade [91,92]; and (d) the additional atoms which the dislocations represent and the expected number of extra vacancies in the bottom 15 nm of the sample relative to the top 10 nm. Note that atomic and vacancy concentrations are given in units of area of basal plane.

In order for the aforementioned Point Defect model to be capable of causing the microstructural changes observed, a sufficient number of point defects must survive the dynamic annealing within the volume affected by each ion induced atomic collision cascade. In particular, vacancies are required both to survive and agglomerate into small loops in sufficient numbers in order to cause the necessary degree of contraction of the basal planes.

Consider a 25 nm thick sample of graphite irradiated to a fluence of 1.2×10^{13} ions cm^{-2} such that a regular array of dislocations has been formed as shown in Figs. 2b and 5c.

Approximating the damage profile shown in Fig. 5a to a simpler step profile with an average of 0.018 DPA in the top 10 nm and 0.026 DPA in the bottom 15 nm as shown in Fig. 5b, the difference of 0.008 DPA will cause a basal plane in the lower region of the sample to have experienced the creation of an additional $3.0{\times}10^{13}$ vacancies cm^{-2} compared to a basal plane in the upper region. Molecular dynamics simulations of atomic collision cascades predict that typically 20% of the point defects created by an atomic collision cascade survive the recombination processes which occur during and immediately after the ballistic and thermal phases [91,92]. Consequently, at this fluence it can be estimated that on average an additional $6.1{\times}10^{12}$ vacancies cm^{-2} remain in each basal plane in the lower region relative to those in the upper region.

As the dislocations in the array shown in Fig. 2b have an average spacing of 500 nm, they represent $1.6{\times}10^{12}$ atoms cm^{-2} in the upper region of the sample which is fewer than the additional $6.1{\times}10^{12}$ vacancies cm^{-2} estimated for the lower region. It is therefore clear that a sufficient number of excess vacancies exist in the lower region of the sample to account for our observations – provided that a significant fraction of them are able to agglomerate to form extended defects and thus cause contraction of the basal planes in the lower region of the film.

As discussed in section 3.5.1, current estimates of the vacancy migration energy in are in the range 1–1.1 eV with historical values from both experimental and theoretical work always yielding values of $\geq$ 1.0 eV [18,77–82]. With a 1.0 eV migration energy [77], on average a vacancy would make one jump per $1.6{\times}10^{3}$ s at room temperature and one jump per $8.0{\times}10^{4}$ s for 1.1 eV [78]. This is clearly insufficient to give rise to significant vacancy agglomeration on the timescale of our experiments which last 600 s. In addition, although thermal spikes have been seen to cause observable effects in dense materials [25,26,28], the dilute nature of the energy deposition process in graphite coupled with the short lifetime (10^{-11} s) of the thermal spike renders any thermal-spike induced vacancy motion also negligible.

The Point Defect model is capable of explaining the experimental results when considering the number of point defects generated under the ion irradiation conditions used. However, the current understanding of vacancy migration mechanisms and energies makes the Point Defect model incompatible with these room temperature observations. Therefore further work is needed on vacancy migration and/or the nature of atomic collision cascades in graphite in order to validate the Point Defect model.

3.7   *Other possible models*

It has been clearly demonstrated in the experiments reported here that dislocations can be

generated in significant concentrations under displacing irradiation and that those dislocations are highly mobile at room temperature. Furthermore, these dislocations are able to agglomerate to form larger structures in the material in the form of kink-bands in our thin foils. Our observations provide evidence supporting the hypothesis that the process is driven by basal-plane contraction in the more heavily damaged region of the foil; a conclusion also reached by Bacon and Rao [90]. Although currently there is no theoretical model capable of predicting these observations from atomistic considerations, it is possible that an explanation may lie in the rucking of basal planes [14] or out-of-plane deformation due to defects [19–24,74–76,93].

3.8   *Comparison to neutron irradiation conditions*

Dimensional change in nuclear graphites is a complex multiscale problem in which the filler, binder, porosity, cracks and atomic-level effects interact within the polygranular structure. The experiments reported here are designed to investigate the effects in a single crystal to give insights into the response of individual grains and the atomistic mechanisms operating within the graphite crystal structure.

The irradiation conditions chosen for the experiments reported here deliberately created a damage profile across the sample thickness which would not be typical of, for example, fast-neutron irradiation. Furthermore, the atomic collision cascade of an energetic heavy-ion is denser than that of an energetic neutron. However, fast-neutrons do give rise to inhomogeneous stresses within the irradiated material [9,94]. The experiments reported here thus serve to explore some of the fundamental mechanisms operating in graphite under displacing irradiation by which inhomogeneous stresses give rise to macroscopic deformation of the material.

At the final fluence of 3.0×10^{13} ions cm^{-2}, the number of irradiation induced displacement events within the sample varied from 0.025 at a depth of 1 nm to 0.071 at 17.5 nm. These are very low damage levels compared to neutron radiation damage studies into dimensional change in graphite which typically explore damage levels starting from those in the current study and up to end-of-life damage levels for graphite in AGRs of 10 DPA [3] and higher [12]. Studies into irradiation damage induced dimensional change have traditionally focused on neutron irradiation at higher temperatures. At the lower temperatures reported in the literature, neutron irradiation of HOPG at 150°C has been shown to demonstrate dimensional change in the a/b-direction of about 0.5% at 0.07 DPA (= 5×10^{19} n cm^{-2}) [95].

18

4.   Summary

High levels of mechanical stress have been induced in thin graphite samples using ion irradiation conditions which produce a damage profile that varies as a function of depth. This damage profile caused significantly different degrees of basal plane contraction at the top and bottom of the sample resulting in a sequence of dramatic microstructural changes including: dislocation production, motion and assembly into defect arrays; kink band network formation with an associated polycrystalline structure; and doming of the sample surface within the polycrystalline grains. The evolution of this dynamic system has been observed using *in situ* TEM revealing previously unknown details of the sequence of structural developments and the physics of the mechanisms driving these complex phenomena. These results provide new experimental data that contributes towards developing an improved understanding of the atomistic mechanism of dimensional change in single crystal graphite.

Acknowledgements

References

[1]   Marsden BJ, Hall GN. Graphite in gas-cooled reactors. Comp Nucl Mater 2012;4:325.

[2]   Guérin Y, Was GS, Zinkle SJ, Editors G. Materials challenges for advanced nuclear energy systems. Mater Res Soc Bull 2009;34:10.

[3]   Was GS. Materials degradation in fission reactors: Lessons learned of relevance to fusion reactor systems. J Nucl Mater 2007;367-370:11.

[4]   Young RJ, Kinloch IA, Gong L, Novoselov KS. The mechanics of graphene nanocomposites: A review. Compos Sci Technol 2012;72:1459.

[5]   Gong L, Young RJ, Kinloch IA, Riaz I, Jalil R, Novoselov KS. Optimizing the reinforcement of polymer-based nanocomposites by graphene. ACS Nano 2012;6:2086.

[6]   Novoselov KS, Fal'ko VI, Colombo L, Gellert PR, Schwab MG, Kim K. A roadmap for graphene. Nature 2012;490:192.

[7]   Georgiou T, Jalil R, Belle BD, Britnell L, Gorbachev R V, Morozov S V, et al. Vertical field-effect transistor based on graphene-WS2 heterostructures for flexible and transparent electronics. Nat Nanotechnol 2013;8:100.

[8]   Haigh SJ, Gholinia A, Jalil R, Romani S, Britnell L, Elias DC, et al. Cross-sectional imaging of individual layers and buried interfaces of graphene-based heterostructures and superlattices. Nat Mater 2012;11:764.

[9]   Brocklehurst JE, Kelly BT. The dimensional changes of highly-oriented pyrolytic graphite irradiated with fast neutrons at 430°C and 600°C. Carbon 1993;31:179.

[10]   Henson RW, Perks AJ, Simmons JHW. Lattice parameter and dimensional changes in graphite irradiated between 300 and 1350°C. Carbon 1968;6:789.

[11]   Marsden BJ, Hall GN, Wouters O, Vreeling JA, van der Laan J. Dimensional and material property changes to irradiated Gilsocarbon graphite irradiated between 650 and 750°C. J Nucl Mater 2008;381:62.

[12]   Perks AJ, Simmons JHW. Dimensional changes and radiation creep of graphite at very high neutron doses. Carbon 1966;4:85.

[13]   Price RJ. High-temperature neutron irradiation of highly oriented carbons and graphites. Carbon 1974;12:159.

[14]   Heggie MI, Suarez-Martinez I, Davidson C, Haffenden G. Buckle, ruck and tuck: A proposed new model for the response of graphite to neutron irradiation. J Nucl Mater 2011;413:150.

[15]   Karthik C, Kane J, Butt DP, Windes WE, Ubic R. In situ transmission electron microscopy of electron-beam induced damage process in nuclear grade graphite. J Nucl Mater 2011;412:321.

[16]   Tsai S-C, Huang E-W, Kai J-J, Chen F-R. Microstructural evolution of nuclear grade graphite induced by ion irradiation at high temperature environment. J Nucl Mater 2013;434:17.

[17]   Burchell TD, Snead LL. The effect of neutron irradiation damage on the properties of grade NBG-10 graphite. J Nucl Mater 2007;371:18.

[18]   Telling RH, Heggie MI. Radiation defects in graphite. Phil Mag 2007;87:4797.

[19]   Banhart F, Kotakoski J, Krasheninnikov A V. Structural defects in graphene. ACS Nano 2011;5:26.

[20]   Cataldo F. The impact of a fullerene-like concept in carbon black science. Carbon 2002;40:157.

[21]   Liu T-H, Gajewski G, Pao C-W, Chang C-C. Structure, energy, and structural transformations of graphene grain boundaries from atomistic simulations. Carbon 2011;49:2306.

[22]   Liu Y, Yakobson BI. Cones, pringles, and grain boundary landscapes in graphene topology. Nano Lett 2010;10:2178.

[23]   Schniepp HC, Kudin KN, Li J-L, Prud'homme RK, Car R, Saville D a, et al. Bending properties of single functionalized graphene sheets probed by atomic force microscopy. ACS Nano 2008;2:2577.

[24]   Yazyev O V., Louie SG. Topological defects in graphene: Dislocations and grain boundaries. Phys Rev B 2010;81:195420.

[25]   Donnelly S, Birtcher R, Templier C, Vishnyakov V. Response of helium bubbles in gold to displacement-cascade damage. Phys Rev B 1995;52:3970.

[26]   Birtcher R, Donnelly S. Plastic Flow Induced by Single Ion Impacts on Gold. Phys Rev Lett 1996;77:4374.

[27]   Donnelly SE, Birtcher RC, Allen CW, Morrison I, Furuya K, Song M, et al. Ordering in a fluid inert gas confined by flat surfaces. Science 2002;296:507.

[28]   Rehn L, Birtcher R, Donnelly S, Baldo P, Funk L. Origin of Atomic Clusters during Ion Sputtering. Phys Rev Lett 2001;87:207601.

[29]   Greaves G, Hinks JA, Busby P, Mellors NJ, Ilinov A, Kuronen A, et al. Enhanced Sputtering Yields from Single-Ion Impacts on Gold Nanorods. Phys Rev Lett 2013;111:065504.

[30]   Donnelly SE, Birtcher RC, Vishnyakov VM, Carter G. Annealing of isolated amorphous zones in silicon. Appl Phys Lett 2003;82:1860.

[31]   Baker C, Kelly A. An electron microscope study of radiation damage in single crystal graphite. Phil Mag 1965;11:729.

[32]   Bollmann W, Hennig GR. Electron microscope observations of irradiated graphite single crystals. Carbon 1964;1:525.

[33]   Heerschap M, Schüller F. Vacancy and Interstitial Loops in Graphite Single Crystals Reactor-Irradiated at 900 and 1200C. Carbon 1969;7:624.

[34]   Hinman GW, Haubold A, Gardner JO, Layton JK. Vacancies and interstitial clusters in irradiated graphite. Carbon 1970;8:341.

[35]   Shtrombakh YI, Gurovich BA, Platonov PA, Alekseev VM. Radiation damage of graphite and carbon-graphite materials. J Nucl Mater 1995;225:273.

[36]   Bacon DJ, Dumler I, Rao AS. The structure of graphite and silicon carbide resulting from helium ion bombardment. J Nucl Mater 1981;103-104:427.

[37]   Borisov a. M, Mashkova ES, Nemov AS, Virgiliev YS. Sputtering of HOPG under high-dose ion irradiation. Nucl Instrum Meth B 2007;256:363.
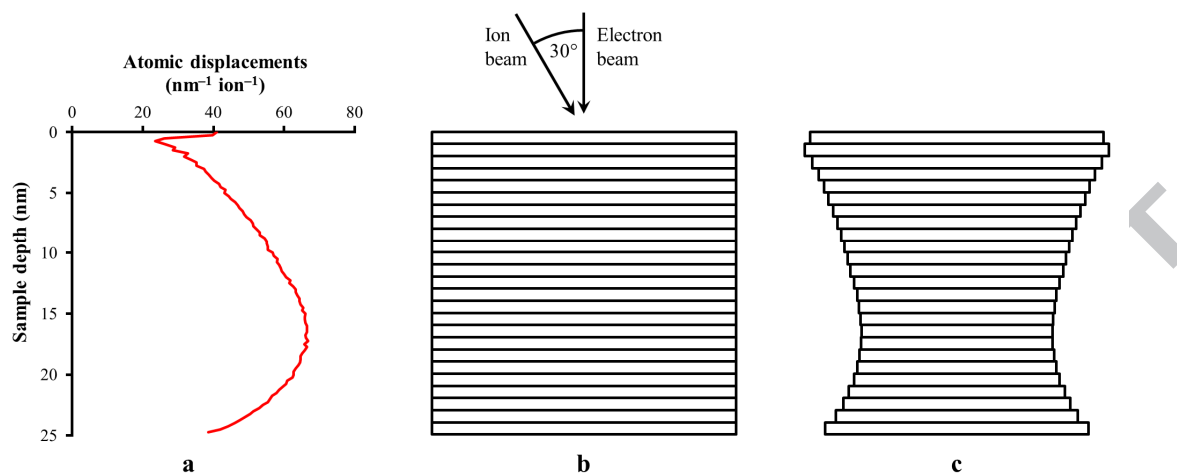
[38] Chernikov VN, Kesternich W, Ullmaier H. Radiation effects and gas cavities in pyrolytic graphite implanted with helium ions. J Nucl Mater 1996;227:157.

[39] Dunlop a., Jaskierowicz G, Chadderton LT. High resolution transmission electron microscopy of GeV heavy ion irradiated graphite. Nucl Instrum Meth B 1998;145:532.

[40] Tanabe T. Radiation damage of graphite - degradation of material parameters and defect structures. Phys Scr 1996;T64:7.

[41] Abe H, Naramoto H, Iwase A, Kinoshita C. Effect of damage cascades on the irradiation-induced amorphization in graphite. Nucl Instrum Meth B 1997;127-128:681.

[42] Abe H, Naramoto H, Kinoshita C. Amorphization of graphite under ion or electron irradiation. Mater Res Soc Proc 2011;373:383.

[43] Kushita KN, Hojou K, Furuno S. Radiation damage of graphite due to hydrogen-ion bombardment at very low temperature. J Nucl Mater 1992;191-194:351.

[44] Kushita KN, Hojou K. In situ EELS observation of graphite structure modification due to hydrogen ion irradiation. Ultramicroscopy 1991;35:289.

[45] Muto S, Tanabe T, Takeuchi M, Kobayashi Y, Furuno S, Hojou K. TEM analyses of surface ridge network in an ion-irradiated graphite thin film. J Nucl Mater 1999;271-272:285.

[46] Koike J, Pedraza DF. Dimensional changes in highly oriented pyrolytic graphite due to electron-irradiation. J Mater Res 2011;9:1899.

[47] Muto S, Tanabe T. Temperature effect of electron-irradiation-induced structural modificcation in graphite. J Nucl Mater 2000;287:917.

[48] Pedraza DF, Koike J. Dimensional changes in grade H-451 nuclear graphite due to electron irradiation. Carbon 1994;32:727.

[49] Ni ZH, Wang HM, Kasim J, Fan HM, Yu T, Wu YH, et al. Graphene thickness determination using reflection and contrast spectroscopy. Nano Lett 2007;7:2758.

[50] Blake P, Hill EW, Castro Neto AH, Novoselov KS, Jiang D, Yang R, et al. Making graphene visible. Appl Phys Lett 2007;91:063124.

[51] Novoselov KS, Geim AK, Morozov S V, Jiang D, Zhang Y, Dubonos S V, et al. Electric field effect in atomically thin carbon films. Science 2004;306:666.

[52] Meyer JC, Girit CO, Crommie MF, Zettl A. Imaging and dynamics of light atoms and molecules on graphene. Nature 2008;454:319.

[53] Casiraghi C. Doping dependence of the Raman peaks intensity of graphene close to the Dirac point. Phys Rev B 2009;80:233407.
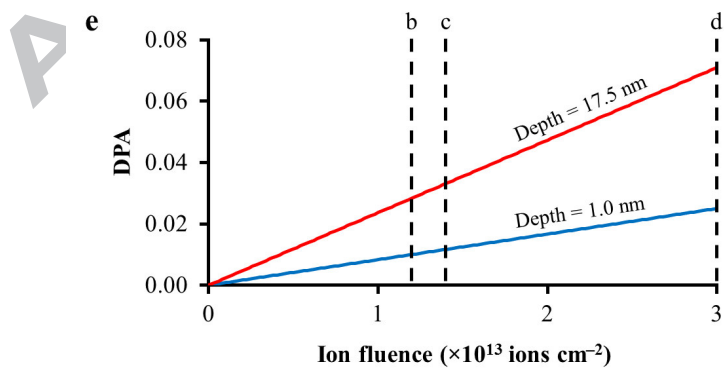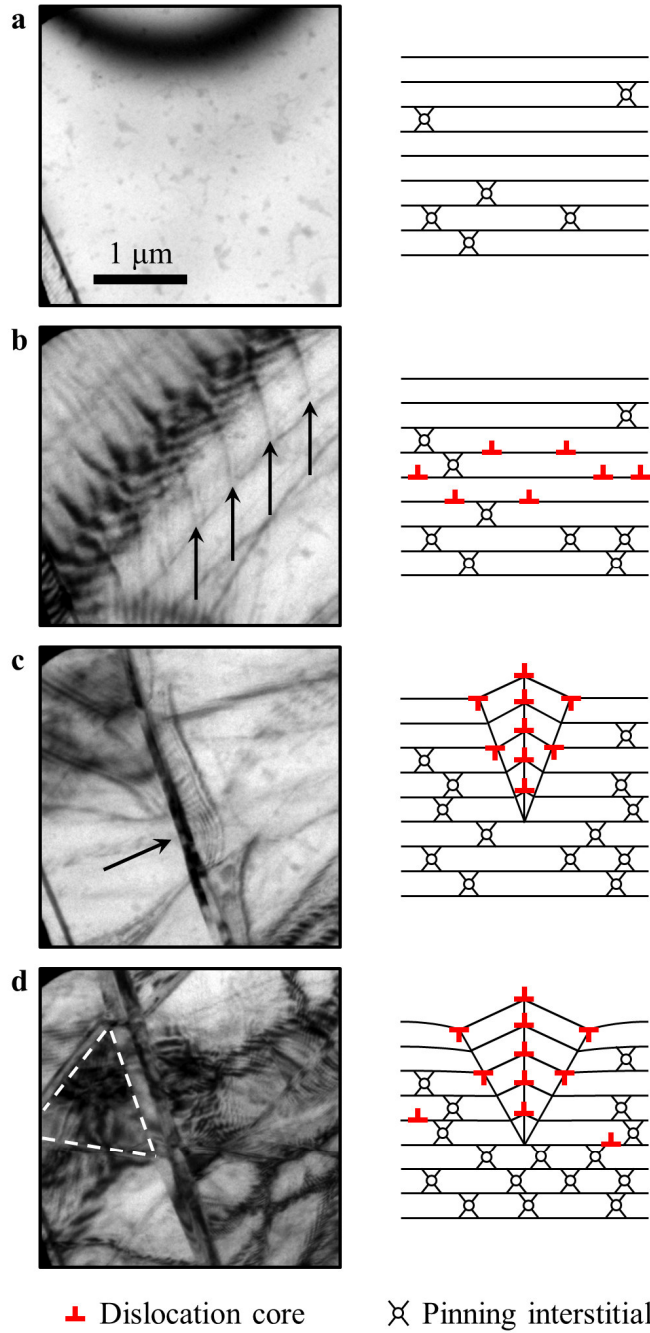
22

[54] Lin Y-C, Lu C-C, Yeh C-H, Jin C, Suenaga K, Chiu P-W. Graphene annealing: how clean can it be? Nano Lett 2012;12:414.

[55] Lin Y-C, Jin C, Lee J-C, Jen S-F, Suenaga K, Chiu P-W. Clean transfer of graphene for isolation and suspension. ACS Nano 2011;5:2362.

[56] Hinks JA, van den Berg JA, Donnelly SE. MIAMI: Microscope and ion accelerator for materials investigations. J Vac Sci Technol A 2011;29:021003.

[57] Koike J, Pedraza D. Structural change of graphite during electron irradiation. Mater Res Soc Proc 1992;279:67.

[58] Ziegler JF, Ziegler MD, Biersack JP. SRIM – The stopping and range of ions in matter (2010). Nucl Instrum Meth B 2010;268:1818.

[59] Kelly BT. Physics of Graphite. Barking, England: Applied Science Publishers; 1981.

[60] Kelly BT, Foreman AJE. The theory of irradiation creep in reactor graphite – The dislocation pinning-unpinning model. Carbon 1974;12:151.

[61] Grenall A. Direct Observation of Dislocations in Graphite. Nature 1958;182:448.

[62] Baker C, Kelly A. The effect of neutron irradiation on the elastic moduli of graphite single crystals. Phil Mag 1964;9:927.

[63] Amelinckx S, Delavignette P. Electron Optical Study of Basal Dislocations in Graphite. J Appl Phys 1960;31:2126.

[64] Amelinckx S, Delavignette P, Heerschap M. Dislocations and stacking faults in graphite. Chem Phys Carbon 1965;1:2.

[65] Delavignette P, Amelinckx S. Dislocation patterns in graphite. J Nucl Mater 1962;5:17.

[66] Thrower PA. The study of defects in graphite by transmission electron microscopy. Chem Phys Carbon 1969;5:217.

[67] Williamson GK. Electron microscope studies of dislocation structures in graphite. Proc R Soc A 1960;257:457.

[68] Barsoum MW, Murugaiah A, Kalidindi SR, Zhen T, Gogotsi Y. Kink bands, nonlinear elasticity and nanoindentations in graphite. Carbon 2004;42:1435.

[69] Niwase K, Tanabe T, Sugimoto M, Fujita FE. Modification of graphite structure by D+ and He+ bombardment. J Nucl Mater 1989;162-164:856.

[70] Freise EJ, Kelly A. Twinning in Graphite. Proc R Soc A 1961;264:269.

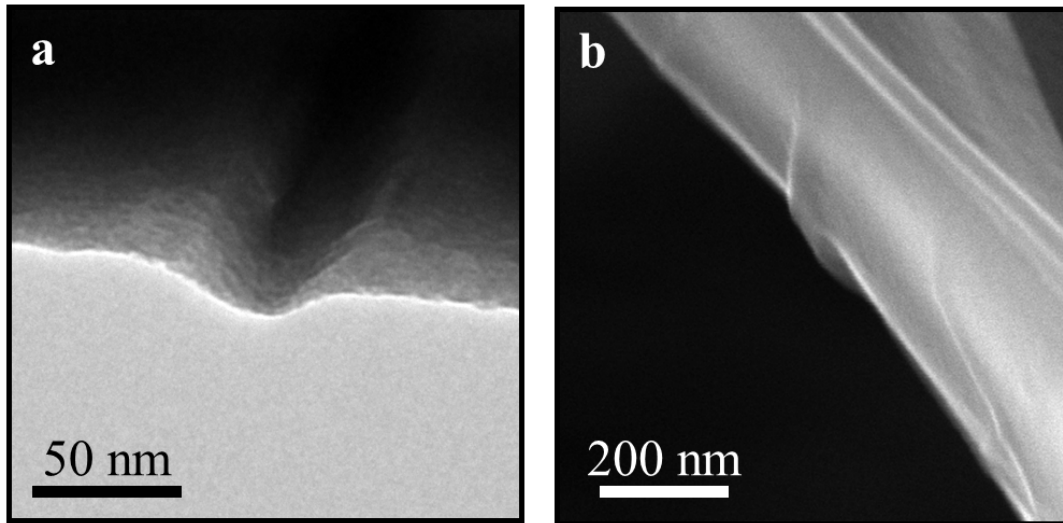[71] Thomas JM, Glenda Hughes EE, Williams BR. Unusual Twinning in Graphite. Nature 1963;197:682.

23

[72] Nabarro FRN, Argon AS. Egon Orowan. 2 August 1902-3 August 1989. Biogr Mem Fellows R Soc 1995;41:316.

[73] Liu Y, Yakobson BI. Cones, pringles, and grain boundary landscapes in graphene topology. Nano Lett 2010;10:2178.

[74] Chen S, Chrzan DC. Continuum theory of dislocations and buckling in graphene. Phys Rev B 2011;84:214103.

[75] Hashimoto A, Suenaga K, Gloter A, Urita K. Direct evidence for atomic defects in graphene layers. Nature 2004;430:17.

[76] Coraux J, N'Diaye AT, Busse C, Michely T. Structural coherency of graphene on Ir(111). Nano Lett 2008;8:565.

[77] Lee G-D, Wang C, Yoon E, Hwang N-M, Kim D-Y, Ho K. Diffusion, coalescence, and reconstruction of vacancy defects in graphene layers. Phys Rev Lett 2005;95:205501.

[78] Latham CD, Heggie MI, Alatalo M, Oberg S, Briddon PR. The contribution made by lattice vacancies to the Wigner effect in radiation-damaged graphite. J Phys Condens Matter 2013;25:135403.

[79] Krasheninnikov AV, Lehtinen PO, Foster AS, Nieminen RM. Bending the rules: Contrasting vacancy energetics and migration in graphite and carbon nanotubes. Chem Phys Lett 2006;418:132.

[80] Kaxiras E, Pandey K. Energetics of defects and diffusion mechanisms in graphite. Phys Rev Lett 1988;61:2693.

[81] El-Barbary A, Telling R, Ewels C, Heggie M, Briddon P. Structure and energetics of the vacancy in graphite. Phys Rev B 2003;68:144107.

[82] Zhang H, Zhao M, Yang X, Xia H, Liu X, Xia Y. Diffusion and coalescence of vacancies and interstitials in graphite: A first-principles study. Diam Relat Mater 2010;19:1240.

[83] Ma Y. Simulation of interstitial diffusion in graphite. Phys Rev B 2007;76:075419.

[84] Lidiard AB, Perrin R. The growth of interstitial clusters in graphite under irradiation. Philos Mag 1966;14:433.

[85] Thrower PA. Interstitial and vacancy loops in graphite irradiated at high temperatures. Brit J Appl Phys 1964;15:1153.

[86] Abrams KJ, Hinks JA, Pawley CJ, Greaves G, van den Berg JA, Eyidi D, et al. Helium irradiation effects in polycrystalline Si, silica, and single crystal Si. J Appl Phys 2012;111:083527.

[87] Mader S, Tu KN. Microstructure of xenon–implanted silicon. J Vac Sci Technol 1975;12:501.

[88] Evans JH. The role of implanted gas and lateral stress in blister formation mechanisms. J Nucl Mater 1978;76-77:228.

[89] Chernikov VN, Kesternich W, Ullmaier H. Radiation effects and gas cavities in pyrolytic graphite implanted with helium ions. J Nucl Mater 1996;227:157.

[90] Bacon DJ, Rao AS. The structure of graphite bombarded with light, gaseous ions. J Nucl Mater 1980;91:178.

[91] Nordlund K, Ghaly M, Averback R, Caturla M, Diaz de la Rubia T, Tarus J. Defect production in collision cascades in elemental semiconductors and fcc metals. Phys Rev B 1998;57:7556.

[92] Borodin VA. Molecular dynamics simulation of annealing of post-ballistic cascade remnants in silicon. Nucl Instrum Meth B 2012;282:33.

[93] Warner JH, Margine ER, Mukai M, Robertson AW, Giustino F, Kirkland AI. Dislocation-driven deformations in graphene. Science 2012;337:209.

[94] Kelly BT. The theory of irradiation damage in graphite. Carbon 1977;15:117.

[95] Kelly BT. Graphite – the most fascinating nuclear material. Carbon 1982;20:3.

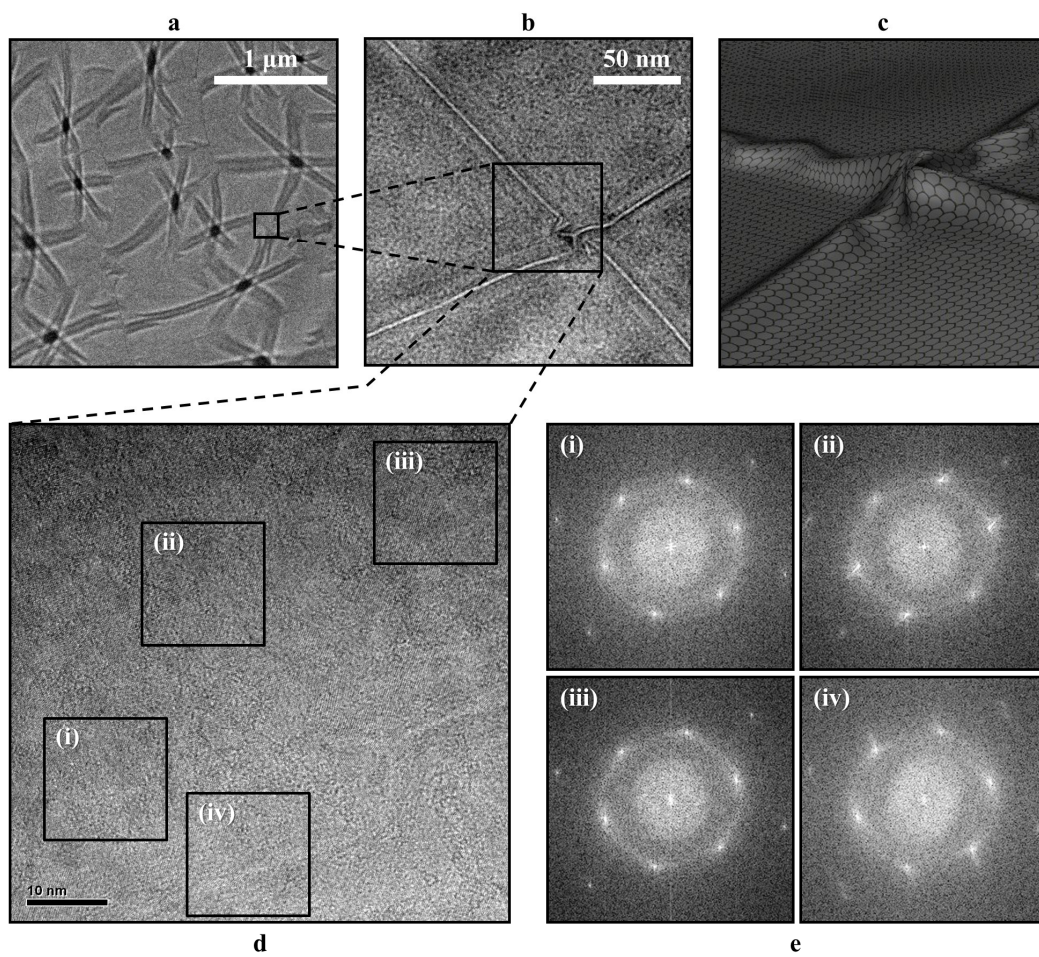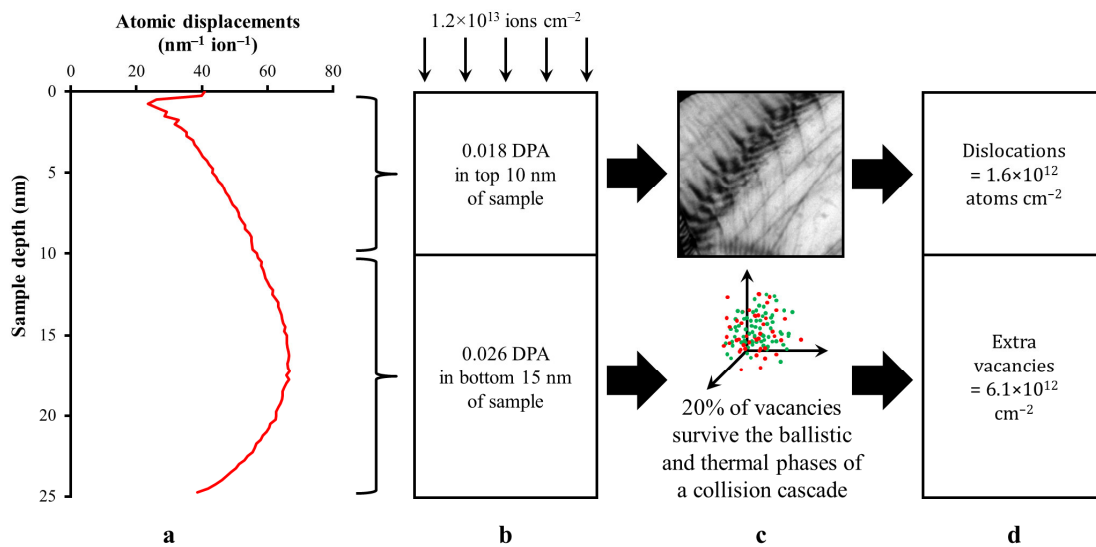**Atomic displacements**
(nm⁻¹ ion⁻¹)

0   20   40   60   80

Sample depth (nm)

0

5

10

15

20

25

a

Ion
beam   30°   Electron
beam

b

c

⊥ Dislocation core   ⋈ Pinning interstitial

27

Atomic displacements (nm⁻¹ ion⁻¹)

1.2×10^{13} ions cm^{-2}

0.018 DPA in top 10 nm of sample

0.026 DPA in bottom 15 nm of sample

20% of vacancies survive the ballistic and thermal phases of a collision cascade

Dislocations = 1.6×10^{12} atoms cm^{-2}

Extra vacancies = 6.1×10^{12} cm^{-2}

a   b   c   d

30